LETTERS
PUBLISHED ONLINE: 3 JUNE 2012 | DOI: 10.1038/NNANO.2012.81
nature nanotechnology

Flexible molecular-scale electronic devices

Sungjun Park[1‡], Gunuk Wang[1†‡], Byungjin Cho[1†], Yonghun Kim[1], Sunghoon Song[1], Yongsung Ji[1], Myung-Han Yoon[1,2] and Takhee Lee[3]*

Flexible materials and devices could be exploited in light-emitting diodes[1], electronic circuits[2,3], memory devices[4], sensors[5,6], displays[7,8], solar cells[9] and bioelectronic devices[10]. Nanoscale elements such as thin films[11,12], nanowires[13], nanotubes[14] and nanoparticles[4] can also be incorporated into the active films of mechanically flexible devices. Large-area devices containing extremely thin films of molecular materials[15,16] represent the ultimate scaling of flexible devices based on organic materials, but the influence of bending and twisting on the electrical and mechanical stability of such devices has never been examined. Here, we report the fabrication and characterization of two-terminal electronic devices based on self-assembled monolayers of alkyl or aromatic thiol molecules on flexible substrates. We find that the charge transport characteristics of the devices remain stable under severe bending conditions (radius $\leq$ 1 mm) and a large number of repetitive bending cycles ($\geq$1,000). The devices also remain reliable in various bending configurations, including twisted and helical structures.

Previously, we fabricated a three-terminal molecular-scale transistor on a rigid substrate[17]. Although three-terminal devices are more versatile than two-terminal devices, device yields have been very low so far[17]. For this reason we chose a two-terminal configuration (Fig. 1) to investigate how the performance of flexible molecular-scale electronic devices changes in response to mechanical deformation. Polyimide (PI) was used as the flexible substrate for two reasons. First, compared with other flexible substrates, it has a relatively high thermal stability (up to 520 K), which prevents substrate deformation during the thermal treatment used to make the isolating layer (photoresist) insoluble in ethanol for the self-assembly process performed on the bottom gold electrode[15]. Second, the low surface roughness of PI reduces the defect density of the self-assembled monolayer (SAM) molecules in the junction. Indeed, atomic force microscopy revealed that the root-mean-square roughness of a 2.5 μm × 2.5 μm region of the surface was ~1.9 Å (Supplementary Fig. S2). Further details on the device fabrication process are provided in the Methods and Supplementary Information.

To prevent electrical shorts due to penetration of the top metal layer during deposition[15,18,19], we introduced a layer of highly conducting polymer, PEDOT:PSS, between the top metal layer and the SAM (as first done by Akkerman *et al.*[15,20]). Changes in the electrical resistance of PEDOT:PSS films on flexible substrates are negligible, and defects or cracks in the PEDOT:PSS/substrate were not observed, even when the substrate was bent to a radius of 5 mm (ref. 21). The PEDOT:PSS electrode therefore demonstrated good bending stability (Supplementary Figs S10 and S11).

Alkanethiol molecules were used in the SAM because these molecules have been extensively investigated for various types of junction platforms and provide good criteria for determining the suitability of the device structure[15,17,18,22–27]. Three types of alkanethiol molecules (of different length) were used: $[HS(CH_3)_7CH_2]$ (denoted C8), $[HS(CH_3)_9CH_2]$ (C10) and $[HS(CH_3)_{11}CH_2]$ (C12). In total, we fabricated 512 devices on 3 cm × 3 cm units (Fig. 1c). We also made 128 devices in which the SAM comprised 2-naphtalenethiol, octanethiol and octanedithiol (Supplementary Fig. S22).

Generally, the main transport mechanism through alkanethiol molecular junctions is off-resonant tunnelling[15,17,18,22–26,28–30], the signatures of which are temperature-independent current–voltage (I–V) characteristics and an exponential dependence of conductance G on molecular length, $G \propto \exp(-\beta_N N)$, where β_N is a decay factor and N is the number of carbon atoms in the alkanethiol molecule (β_N can be determined from plots of G versus N). To verify tunnelling in our flexible molecular devices, we investigated the current densities J of molecular junctions in a flat substrate (defined as bending radius = ∞) as a function of the number of carbon atoms and temperature T. Figure 1d,e shows the exponential length-dependent and temperature-independent current densities of alkanethiol (C8, C10 and C12) molecular junctions under flat conditions, which are indicative of tunnelling through a molecular tunnel barrier[15,17,18,22–26,28–30]. The error bars in Fig. 1d represent the standard deviation of many junctions (more than ~20 devices for each molecular type). The value of β_N was $0.76 \pm 0.28\ C^{-1}$, which is in good agreement with the reported values of alkyl molecular junctions (Supplementary Figs S7, S8, Table S1).

To ensure a practical device platform, the stability and device lifetime of the molecular junctions must be determined[15,31,32]. Figure 2a,b shows the J–V characteristics (Fig. 2a) and stability (Fig. 2b) of C8, C10 and C12 molecular junctions under flat substrate conditions. The J values were maintained for 1×10^4 s, which indicates that significant deterioration did not occur in the junctions under repeated voltage stress conditions. Two voltage step conditions with short time intervals ($\Delta t = 10$ s) were also applied to test the retention of a C12 molecular junction (Fig. 2c)[26]. The J values were measured at 0.8 V and −0.8 V for 1×10^4 s at $\Delta t = 10$ s, and were retained without significant degradation. These results demonstrate that our molecular device has excellent operational stability and durability (Supplementary Fig. S9).

Bending stability is an important factor affecting the suitability of molecular devices for applications in flexible electronic devices. Accordingly, bending tests were carried out using semicircular cylinders with different bending radii of curvature (10 mm and 5 mm) and under repeated cycles (Supplementary Movie S1). Figure 3a shows current densities J at 0.8 V for C8, C10 and C12 flexible molecular devices with different bending radii (∞, 10 mm and 5 mm); the J values did not change, regardless of the bending radius of curvature, indicating excellent bending stability. Furthermore, up to 1,000 cycles of repetitive bending tests were

[1]School of Materials Science and Engineering, Gwangju Institute of Science and Technology, Gwangju 500-712, Korea, [2]Department of Nanobio Materials and Electronics, Gwangju Institute of Science and Technology, Gwangju 500-712, Korea, [3]Department of Physics and Astronomy, Seoul National University, Seoul 151-747, Korea; [†]Present address: Department of Chemistry and the Smalley Institute for Nanoscale Science and Technology, Rice University, Houston, Texas 77005, USA (G.W.); Department of Mechanical and Aerospace Engineering, University of California, Los Angeles, California 90095, USA (B.C.); [‡]These authors contributed equally to this work. *e-mail: tlee@snu.ac.kr

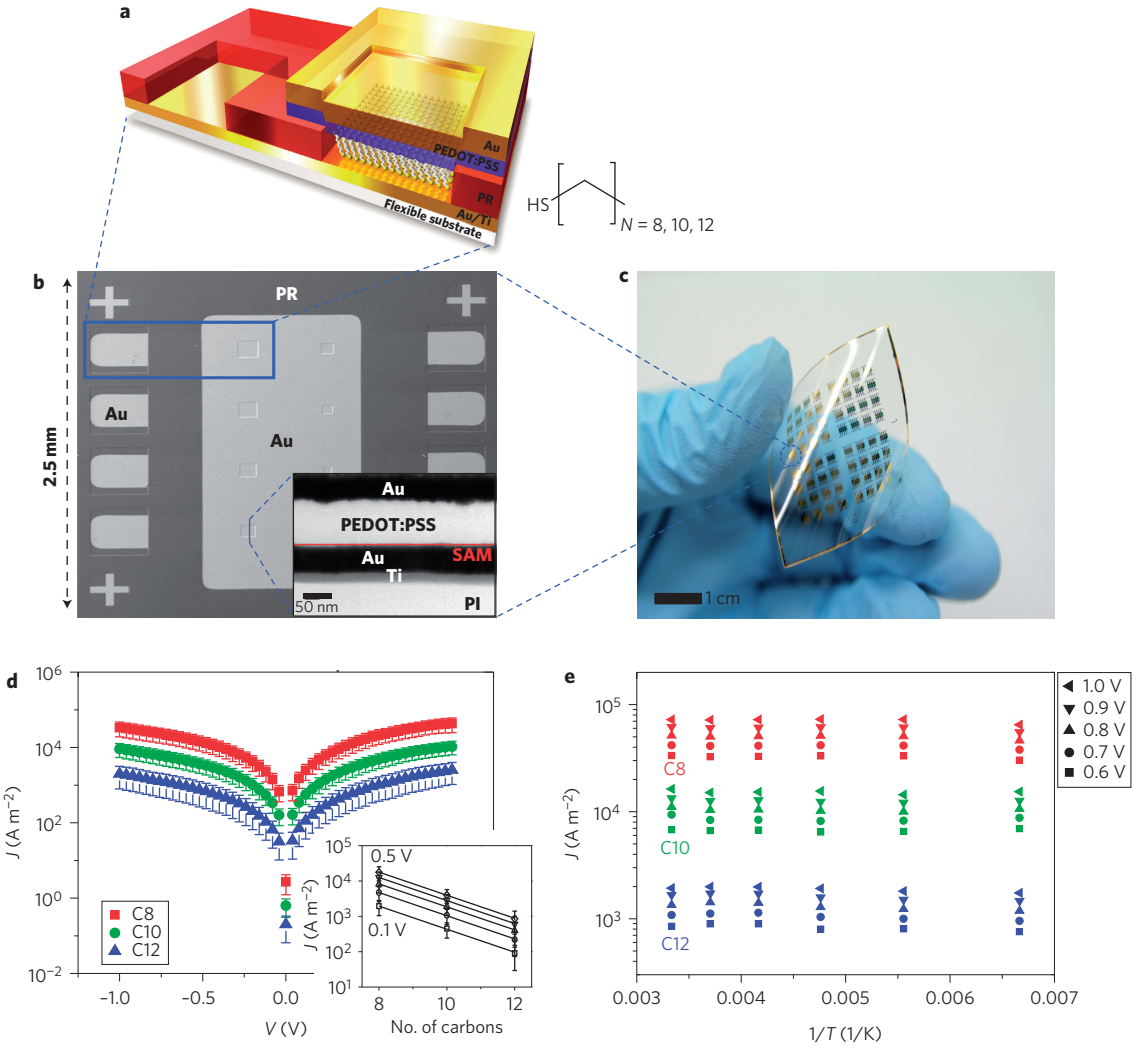

Figure 1 | Molecular devices and electrical characteristics under flat conditions. a, Schematic of a flexible molecular device. The layers (from bottom to top) are a flexible substrate, a bottom gold/titanium electrode, a molecular layer or photoresist (PR) for electrical isolation, a PEDOT:PSS layer and a top gold electrode. **b**, SEM image of a molecular device. The junctions are square-shaped and have sides with lengths ranging from 30 to 100 μm in increments of 10 μm. Inset: high-resolution cross-sectional TEM image of a molecular device. **c**, Photograph of completed device. **d**, Current density *J* (on a log scale) versus voltage *V* for C8, C10 and C12 molecular devices under flat conditions at 300 K. Inset: *J* (on a log scale) versus number of carbon atoms. Error bars denote standard deviation of individual measurements for several devices. **e**, Arrhenius plot (*J* versus inverse temperature) for C8, C10 and C12 molecular devices at different temperatures (from 150 to 300 K) and five different voltages.

performed to verify the flexibility endurance of our devices (Fig. 3b and Supplementary Figs S12–S16).

To prove the operational stability of the flexible molecular devices, we characterized C12 devices under two different bending conditions (tensile and compressive bending). The C12 devices were bent gradually with a vernier calliper (Fig. 3c,f), and the *J* values remained approximately constant during both the tensile and compressive deformations (Fig. 3d,g, Supplementary Fig. S19), indicating the excellent operational stability and durability of our devices under bending.

To prove that a tunnelling transport mechanism was relevant under bent conditions, we performed temperature-variable *J*–*V* measurements on C12 flexible molecular devices under tensile and compressive deformation with a bending radius of 5 mm (Fig. 3e,h). The *J*–*V* characteristics showed temperature-independent behaviour for both cases, indicative of tunnelling through a molecular barrier at temperatures ranging from 150–300 K.

Excellent retention characteristics were achieved, even under severe bending conditions. As shown in Fig. 4a, the *J* values of our flexible molecular devices were maintained when bent over a toothpick (bending radius ≈ 1 mm) for 1×10^4 s, indicating excellent durability and operational stability under extreme bending conditions (Supplementary Fig. S20). These results also suggest that there were no significant changes in the structure and phase of SAM molecules in the molecular junctions when the device was bent severely. We also measured the *J*–*V* characteristics of our flexible molecular devices under various bending configurations. Figure 4b presents the *J*–*V* characteristics and operational stability of C8, C10 and C12 flexible molecular devices under twist conditions. Noticeable degradation was not observed as the twist angle was varied from 0 to 35° (in steps of 5°) (Supplementary Fig. S21). Figure 4c shows a photographic image of the flexible molecular device (a strip with dimensions of 0.25 cm × 40 cm containing 1,024 molecular junctions) rolled over a tube (radius, 2.5 mm) in a helical configuration ($\theta = 30°$). The *J*–*V* characteristics of a C12 device under helical and flat conditions are shown in Fig. 4d. Pronounced changes in these characteristics were not observed under helical structural conditions.

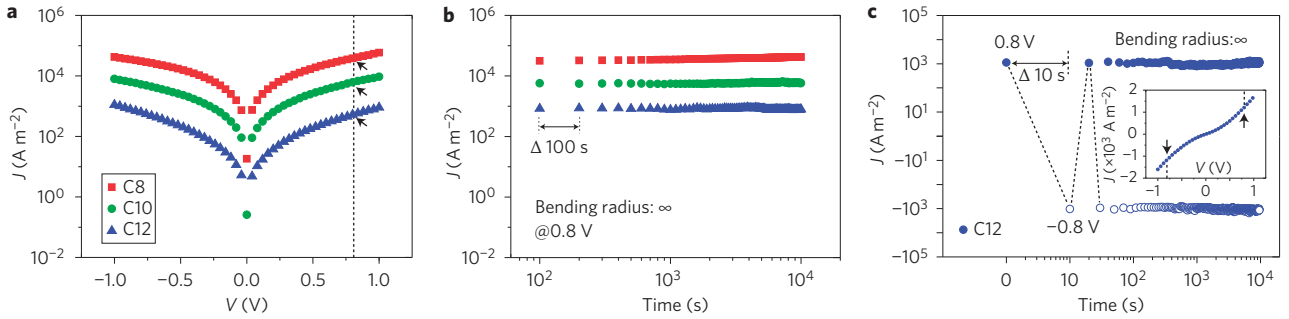

Figure 2 | Stability and retention characteristics of flat devices. a, Representative plots of current density *J* (on a log scale) versus voltage *V* for flat C8, C10 and C12 molecular devices at 300 K. Black arrows indicate current density measured at 0.8 V. **b**, *J* versus time (both on log scales) for flat C8, C10 and C12 devices. *J* was measured every 100 s up to 10,000 s. **c**, *J* versus time (both on log scales) for a flat C12 device measured every 10 s at +0.8 V and −0.8 V. Inset: *J*–*V* curve measured before the retention test (black arrows indicate current density measured at ±0.8 V).

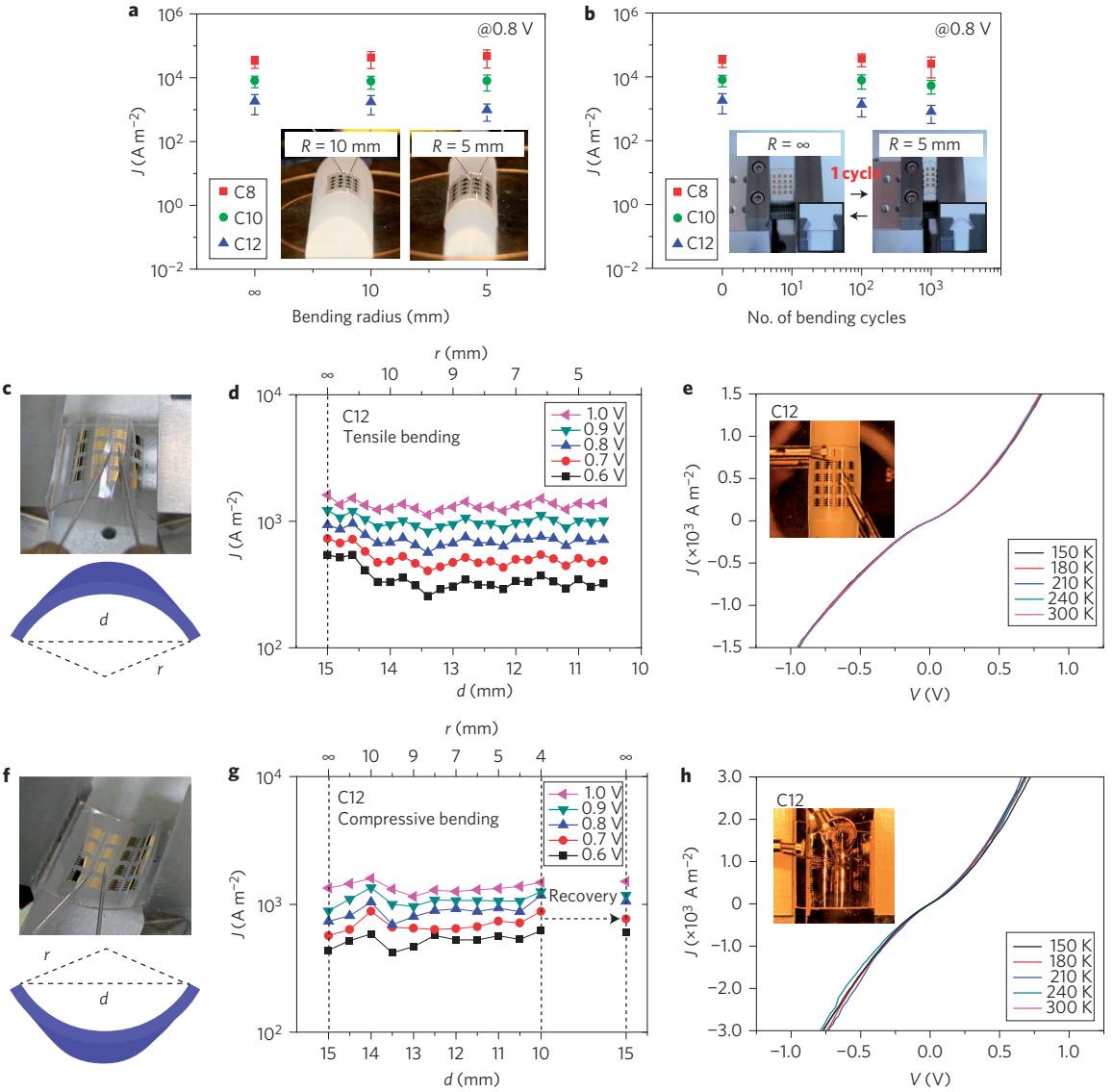

Figure 3 | Bending tests for flexible molecular devices. a,**b**, Current density *J* (on a log scale) at 0.8 V for C8, C10 and C12 devices for three values of bending radius *r* (∞, 10 mm, 5 mm, **a**) and three numbers of bending cycles (0, 100, 1,000, **b**). Insets: devices during the tests. Error bars denote standard deviation of individual measurements of several devices. **c**–**h**, Effects of tensile and compressive bending. Optical images and schematic diagrams of the tensile (**c**) and compressive (**f**) substrates. Bending radius *r* can be determined by measuring the width of the arc, *d* (Supplementary Figs S17, S18). *J* values of the C12 devices at five different voltages as a function of *d* (bottom axis) and *r* (top axis) under tensile (**d**) and compressive (**g**) bending. Current density *J* (on a linear scale) versus *V* for C12 devices at five different temperatures with tensile bending with $r = 5$ mm (**e**) and compressive bending with $r = 5$ mm (**h**). Insets: photographs of devices in a cryostat.

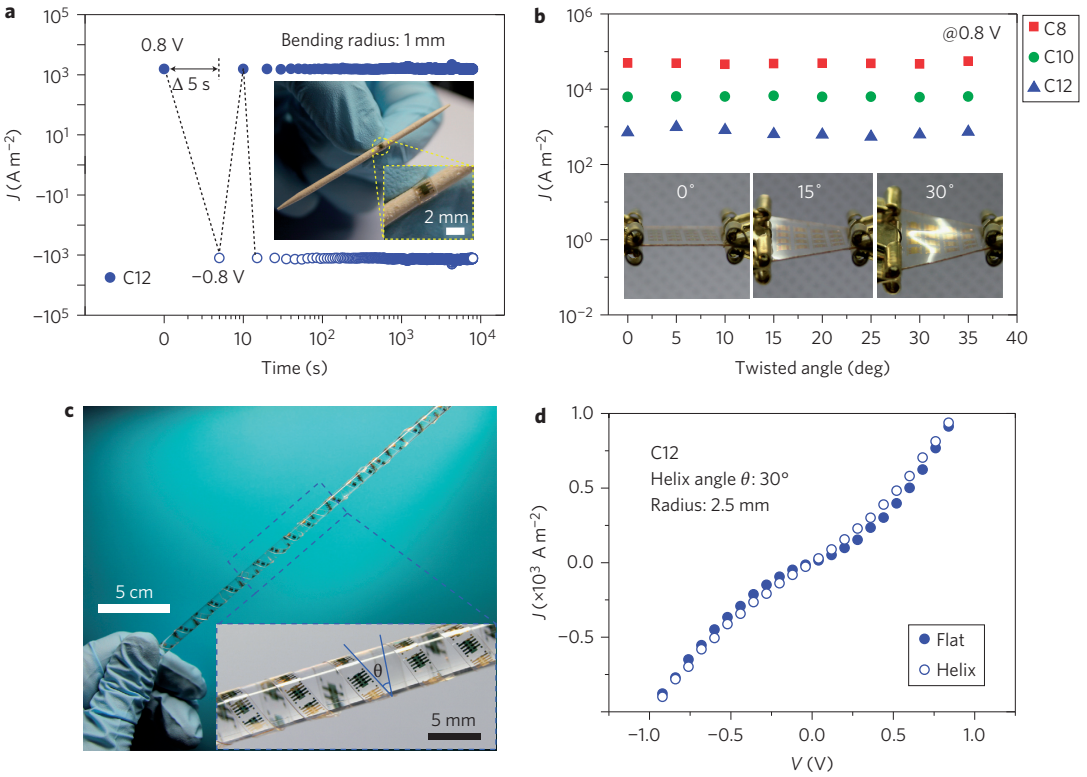

Figure 4 | Flexible molecular devices under twisted and helical conditions. a, Current density *J* versus time (both on log scales) for a C12 device being bent around a toothpick (bending radius, $r \approx 1$ mm, shown in inset). The voltage was stepped between +0.8 V and −0.8 V and *J* was measured every 5 s for 10,000 s. **b**, Values of *J* measured at 0.8 V for C8, C10 and C12 devices as a function of twist angle. Insets: photographs taken at three different angles. **c**, Photograph of flexible devices rolled over a tube (radius, 2.5 mm; $\theta = 30°$) under helical structural conditions. **d**, Plot of *J* (on a linear scale) versus *V* for a C12 device under flat (solid circles) and helical (open circles) conditions.

By demonstrating that ultrathin molecular-monolayer-based devices can operate reliably when bent, twisted or deformed into helical structures, and that their performance can be explained by molecular modelling (see Supplementary Information), our results strongly suggest that it should be possible to make large-area flexible devices in which the active layer is a single layer of molecules.

Methods

Deposition of metal electrode. The patterned bottom gold (50 nm)/titanium (10 nm) and top gold (50 nm) electrodes were formed using shadow masks and an electron-beam evaporator at a pressure of $\sim 1 \times 10^{-7}$ torr and a deposition rate of ~ 0.2 Å s^{-1}.

Formation of self-assembled monolayer. Three different alkyl solutions (concentration, 5 mM) were prepared by adding alkanethiols to 10 ml anhydrous ethanol (Aldrich). Alkanethiol or 2-napthelenethiol SAMs were formed on the exposed gold bottom electrode in a nitrogen-filled glovebox with an oxygen level less than ~10 ppm and an incubation time of 1–2 days by dipping in solution or evaporating solution in a desiccator. Subsequently, the devices were thoroughly rinsed with ethanol to remove any remaining unbound molecules.

Deposition of conducting polymer. PEDOT:PSS (PH 1000 from CLEVIOS, 700 S cm^{-1}) with 5% poly(3,4-ethylene-dioxythiophene) was spin coated (thickness, ~100 nm) on top of the SAM at 3,500 r.p.m. for 30 s. To ensure good contact with the hydrophobic SAM molecules, ~1% non-ionic surfactant (*t*-Oct-C_6H_4-$(OCH_2CH_2)_x$OH from Triton X-100) was added to the PEDOT:PSS solution before spin coating. After deposition of PEDOT:PSS, the devices were dried in a nitrogen-filled glovebox for 2 h.

Microscopic characterization. Molecular devices fabricated on the PI substrate (Neopulim L-3430, MGC) were coated with a thin layer of platinum (thickness, 5 nm) before imaging with a transmission electron microscope (TEM). The top of the samples was characterized by a field-emission scanning electron microscope (FESEM: JEOL JSM-7500F, 5 kV), and cross-sectional images of the device were characterized by TEM (HD-2300A, 200 kV). For TEM observations, the device was prepared using a focused ion beam (Helios Nanolab, 30 kV).

Electrical measurement. *I–V* measurements were performed using a semiconductor parameter analyser (Agilent, B1500A) under ambient conditions. *I–V* measurements were also performed in a liquid nitrogen-cooled cryostat at temperatures ranging from 150 K to room temperature, and retention tests were performed under vacuum. Data obtained from retention and cryostat tests were recorded using a Keithley 4200 source meter.

Bending stability test. Bending tests (Fig. 3a) were carried out using semicircular polyethylene cylinders with different bending radii of curvature (10 mm and 5 mm). For the repetitive bending cycling test (Fig. 3b), the flexible molecular devices were tested on an automated bending machine (Supplementary Movie S1). The degree of bending was controlled using a light-detecting sensor. A toothpick with a bending radius of curvature of 1 mm was used for the extreme bending test.

Received 14 February 2012; accepted 25 April 2012; published online 3 June 2012

References

1. Gustafsson, G. *et al.* Flexible light-emitting diodes made from soluble conducting polymers. *Nature* **357,** 477–479 (1992).
2. Klauk, H., Zschieschang, U., Pflaum, J. & Halik, M. Ultralow-power organic complementary circuits. *Nature* **445,** 745–748 (2007).
3. Sekitani, T., Zschieschang, U., Klauk, H. & Someya, T. Flexible organic transistors and circuits with extreme bending stability. *Nature Mater.* **9,** 1015–1022 (2010).
4. Kim, S. J. & Lee, J. S. Flexible organic transistor memory devices. *Nano Lett.* **10,** 2884–2890 (2010).
5. Sekitani, T. *et al.* Organic nonvolatile memory transistors for flexible sensor arrays. *Science* **326,** 1516–1519 (2009).
6. Mannsfeld, S. C. B. *et al.* Highly sensitive flexible pressure sensors with microstructured rubber dielectric layers. *Nature Mater.* **9,** 859–864 (2010).
7. Gelinck, G. H. *et al.* Flexible active-matrix displays and shift registers based on solution-processed organic transistors. *Nature Mater.* **3,** 106–110 (2004).
8. Sekitani, T. *et al.* Stretchable active-matrix organic light-emitting diode display using printable elastic conductors. *Nature Mater.* **8,** 494–499 (2009).

9. De Arco, L. G. *et al.* Continuous, highly flexible, and transparent graphene films by chemical vapor deposition for organic photovoltaics. *ACS Nano* **4,** 2865–2873 (2010).
10. Kim, D-H. *et al.* Dissolvable films of silk fibroin for ultrathin conformal bio-integrated electronics. *Nature Mater.* **9,** 511–517 (2010).
11. Bae, S. *et al.* Roll-to-roll production of 30-inch graphene films for transparent electrodes. *Nature Nanotech.* **5,** 574–578 (2010).
12. Zhu, Y., Sun, Z. Z., Yan, Z., Jin, Z. & Tour, J. M. Rational design of hybrid graphene films for high-performance transparent electrodes. *ACS Nano* **5,** 6472–6479 (2011).
13. Takei, K. *et al.* Nanowire active-matrix circuitry for low-voltage macroscale artificial skin. *Nature Mater.* **9,** 821–826 (2010).
14. Sun, D-M. *et al.* Flexible high-performance carbon nanotube integrated circuits. *Nature Nanotech.* **6,** 156–161 (2011).
15. Akkerman, H. B., Blom, P. W. M., de Leeuw, D. M. & de Boer, B. Towards molecular electronics with large-area molecular junctions. *Nature* **441,** 69–72 (2006).
16. Van Hal, P. A. *et al.* Upscaling, integration and electrical characterization of molecular junctions. *Nature Nanotech.* **3,** 749–754 (2008).
17. Song, H. *et al.* Observation of molecular orbital gating. *Nature* **462,** 1039–1043 (2009).
18. Kim, T-W., Wang, G., Lee, H. & Lee, T. Statistical analysis of electronic properties of alkanethiols in metal–molecule–metal junctions. *Nanotechnology* **18,** 315204 (2007).
19. Walker, A. V. *et al.* The dynamics of noble metal atom penetration through methoxy-terminated alkanethiolate monolayers. *J. Am. Chem. Soc.* **126,** 3954–3963 (2004).
20. Akkerman, H. B. *et al.* Electron tunneling through alkanedithiol self-assembled monolayers in large-area molecular junctions. *Proc. Natl Acad. Sci. USA* **104,** 11161–11166 (2007).
21. Cho, C-K. *et al.* Mechanical flexibility of transparent PEDOT:PSS electrodes prepared by gravure printing for flexible organic solar cells. *Sol. Energy Mater. Sol. Cells* **95,** 3269–3275 (2011).
22. Cui, X. D. *et al.* Making electrical contacts to molecular monolayers. *Nanotechnology* **13,** 5–14 (2002).
23. Wang, W., Lee, T. & Reed, M. A. Mechanism of electron conduction in self-assembled alkanethiol monolayer devices. *Phys. Rev. B* **68,** 035416 (2003).
24. Engelkes, V. B., Beebe, J. M. & Frisbie, C. D. Length-dependent transport in molecular junctions based on SAMs of alkanethiols and alkanedithiols: effect of metal work function and applied bias on tunneling efficiency and contact resistance. *J. Am. Chem. Soc.* **126,** 14287–14296 (2004).
25. Beebe, J. M., Kim, B., Frisbie, C. D. & Kushmerick, J. G. Measuring relative barrier heights in molecular electronic junctions with transition voltage spectroscopy. *ACS Nano* **2,** 827–832 (2008).
26. Wang, G., Kim, Y., Choe, M., Kim, T-W. & Lee, T. A new approach for molecular electronic junctions with a multilayer graphene electrode. *Adv. Mater.* **23,** 755–760 (2011).
27. Kim, Y. *et al.* Conductance and vibrational states of single-molecule junctions controlled by mechanical stretching and material variation. *Phys. Rev. Lett.* **106,** 196804 (2011).
28. Nitzan, A. & Ratner, M. A. Electron transport in molecular wire junctions. *Science* **300,** 1384–1389 (2003).
29. Akkerman, H. B. & de Boer, B. Electrical conduction through single molecules and self-assembled monolayers. *J. Phys. Condens. Matter* **20,** 013001 (2008).
30. Monnell, J. D. *et al.* Relative conductances of alkaneselenolate and alkanethiolate monolayers on Au{111}. *J. Phys. Chem. B* **109,** 20343–20349 (2005).
31. Green, J. E. *et al.* A 160-kilobit molecular electronic memory patterned at 10^{11} bits per square centimetre. *Nature* **445,** 414–417 (2007).
32. Nijhuis, C. A., Reus, W. F. & Whitesides, G. M. Molecular rectification in metal–SAM–metal oxide–metal junctions. *J. Am. Chem. Soc.* **131,** 17814–17827 (2009).

Acknowledgements

This work was supported by the National Research Laboratory programme and a Korean National Core Research Centre grant from the Korean Ministry of Eduoation, Science and Technology, and the Research Settlement Fund for new faculty at Seoul National University. The authors thank J-S. Yeo, Y. Gon and S-Y. Lee for experimental assistance.

Author contributions

T.L. planned and supervised the project. S.P. designed and performed the experiments. S.P., G.W., B.C. and T.L. analysed and interpreted the data and wrote the manuscript. Y.K. and S.S. assisted in device fabrication and measurements. Y.J. assisted in the bending experiments. M-H.Y. contributed to discussions throughout the project.

Additional information

The authors declare no competing financial interests. Supplementary information accompanies this paper at www.nature.com/naturenanotechnology. Reprints and permission information is available online at http://www.nature.com/reprints. Correspondence and requests for materials should be addressed to T.L.